KSME

Springer

Journal of Mechanical Science and Technology 38 (9) 2024

Original Article
DOI 10.1007/s12206-024-0827-0

Keywords:
· Shape optimization
· Wheel wear
· Dynamics performance
· Wheel-rail interaction
· Geometric profile

Correspondence to:
Bing Yi
bingyi@csu.edu.cn

Citation:
Liu, L., Yi, B., Shi, X., Peng, X. (2024). Kriging-PSO-based shape optimization for railway wheel profile. Journal of Mechanical Science and Technology 38 (9) (2024) 4921~4932.
http://doi.org/10.1007/s12206-024-0827-0

Received February 26th, 2024
Revised April 25th, 2024
Accepted May 14th, 2024

† Recommended by Editor Hyun-Gyu Kim

Kriging-PSO-based shape optimization for railway wheel profile

Long Liu[1], Bing Yi[1], Xiaofei Shi[2] and Xiang Peng[3]

[1]School of Traffic and Transportation Engineering, Central South University, Changsha, China, [2]Guangzhou Railway (Group) Company, Guangzhou Multiple Depot, Guangzhou, China, [3]College of Mechanical Engineering, Zhejiang University of Technology, Hangzhou, China

Abstract The reduction of wheel-rail wear is a fundamental task in railway engineering that significantly affects the operating performance in the lifecycle. To improve the dynamic response and profile wear evolution performance of wheel-rail interaction, a shape optimization procedure for the railway wheel profile is proposed. First, the geometry modeling method, which ensures the continuity of first-order derivation of the wheel profile, is introduced to generate a large number of candidate profiles, and multibody dynamics simulation is conducted to analyze the dynamics response of the wheel profiles, including wear index, lateral force, lateral acceleration of the frame and derailment coefficient. Then, the Kriging model is constructed to establish the relationship between the design variables and objectives obtained by multibody dynamics simulation, and particle swarm optimization (PSO) is employed to evaluate the optimal parameters for wheel profile that simultaneously considers wheel wear, stability, and lateral force. Finally, the performance of the wheel-rail interaction is evaluated to demonstrate the effectiveness of the proposed method. The numerical simulation result indicates that the optimized wheel profile not only has good performance, including contact state, pressure, and friction at the design stage, but also the physical performance is acceptable after a long-term profile evolution during service, which the maximum wear depth of the optimal wheel profile averagely decreases over 10 % in long-term wear evolution.

1. Introduction

As the electric multiple unit train develops towards high-speed and heavy-duty in China, which causes the wheel-rail wear phenomenon to get more and more severe, with a maintenance cost of wheel and rail over billions of dollars [1]. If the geometry of the wheel cannot suitably match the rail profile, abnormal profile wear will occur, which not only leads to high cost for reprofiling and grinding, worsens the wheel-rail contact relationship, and also decreases the running stability and safety, reducing the life cycle of the wheel-rail system [2-5].

The wheel-rail profile matching analysis is a long-standing and still challenging topic in railway engineering, which directly affects the operation performance, cost and safety of a service train. Compared to optimizing the rail profile, wheel profile optimization is more acceptable and easier to conduct in the industry; even if the wheel is in service, the modification can be implemented in the reprofiling cycle [6, 7]. Hence, wheel profile optimization at the design and service stages has drawn much attention.

Wheel profile optimization can be broadly summarized into two categories: reverse shape design and top-down shape design. The former, the reverse design method, uses the wheel-rail contact parameters such as rolling radii difference and contact angle to inversely construct the optimal wheel profile shape. Markine et al. [8] proposed an inverse wheel profile design method by minimizing the difference between the target rolling radii difference function and the optimal one. Shevtsov et al. [9] designed the wheel profile shape by considering rolling contact fatigue and profile wear. A similar profile design method was proposed by Jahed et al. [10], which developed computation efficiency by reducing the design variables. Shen et al. [11] pro-

posed a target-oriented method for wheel profile design based on the contact angle function between the wheel and rail. Based on the field measurement and numerical analysis [12], Ren et al. optimized the S1002 profile to mitigate the flange wear and improve the vehicle curving performance by minimizing the rolling radius difference of the desired and design one. In Ref. [13], Polach proposed a wheel profile design method to satisfy target conicity and wide tread wear spreading. The reverse problem can be efficiently solved as the design variables of the objective function are limited; however, the forthcoming drawback is that the optimal wheel profile cannot ensure an acceptable dynamics performance of a service train as the optimization objective is simple [14]. In the meantime, it is fairly troublesome to determine the target function curve.

Compared with the reverse shape design methods, the top-down shape design pipeline is more convenient to implement. A direct optimization method for wheel profile by minimizing the wheel/rail normal gap at contact points was proposed by Cui et al. [15], which decreases the contact mechanics and improves the performance of curve negotiation; however, the imposed objective function introduces numerous constraints to ensure the monotonicity and convexity of the profile curve with a gradient-based method, which easily sinks into local optimal and cannot ensure a global optimal solution. To develop the degree of conformity between the wheel and rail profiles, Zhang et al. [16] adopted the partial rail expansion method for wheel profile optimization, which can be applied for metro train and railway freight cars with low running speeds. Qi et al. [17] introduced a rotary-scaling fine-tuning method to fine-tune metro wheel profiles by combining radial basis function and particle swarm optimization, which improves the wheel-rail contact relationship for metro trains. Lin et al. [18] proposed using the non-uniform rational B-spline method to optimize the LM wheel profile by considering the geometrical characteristic of the wheel shape, which improves the operation safety and material removal of the wheel. In Ref. [19], Ye et al. presented a wheel profile fine-tuning framework based on radial basis function and particle swarm optimization, which realizes multi-objective including profile wear reduction, improvement of the shape stability, hunting stability, and derailment safety. Due to limited length of the article, interested readers can refer to Refs. [20-24]. Overall, the top-down design method can effectively design a wheel profile to some extent; nevertheless, there are still many difficult challenges such as curve fitting error, profile smoothness, and manufacturability of the optimized wheel shape.

With an insight into shape optimization, we attempted to optimize the geometry parameters of the wheel profile to reduce the numbers of design variables and ensure the smoothness and manufacturability of the optimized wheel profile. Taking the LMA wheel profile as the example generally used in Chinese high-speed trains, it has attracted much attention to reduce profile wear [7, 25], contact stress [15, 26], and develop lateral stability [1], and other dynamics indicators [27]. However, the current methods mainly focus on dynamics performance of the wheel profile on tangent line at the design stage; only a few papers simply validate the dynamics performance on the curved line, which does not directly consider the dynamics performance of the wheel profile on both the tangent and curve lines. In addition, even though much progress has been made for wheel profile optimization, how to combine surrogate model and optimization method to efficiently and reliably design wheel profile remains to be further investigated. The above-mentioned challenges urge this paper to establish the dynamics response of the wheel-rail system and the geometry parameters, considering dynamic behavior on both the tangent and curve lines by using the kriging model and the weighted particle swarm optimization method to obtain the optimal wheel profile, of which the dynamics performance is improved compared to LMA profile.

The rest of this paper is organized as follows: Sec. 2 describes the geometry modeling method for wheel profile. The objective formulation and optimization procedure are detailed in Sec. 3. In Sec. 4, the numerical analysis for the optimal result is conducted. Sec. 5 summarizes the proposed shape optimization procedure for the railway wheel profile.

2. Parametric modeling of wheel profile

The geometry of the wheel profile is constructed with multiple arcs and straight lines, as shown in Fig. 1. Compared with the shape-fitting method for wheel profile representation, the primary benefit of the arcs-lines-based shape descriptor is that it ensures the smoothness of the wheel profile without additional constraints. Additionally, it is easy to manufacture and maintain, resulting in cost savings and a fast production time. Therefore, parametric modeling for wheel profiles is utilized for shape optimization.

The main area for contact with the rail is constructed with three arcs and a straight line; thus we attempt to optimize this area to obtain an optimal wheel profile which is of good performance on wheel-rail contact. The design variables of the optimization issue are the radii r_1, r_2, and r_3, as well as slope degree N, and the abscissa of tangent point t_x.

The start point S is set at the point with the maximum contact angle of the wheel and the end point E is on the straight line and its abscissa is 30 mm [15]. The slopes of the points S and E are given in Eq. (1); please note that l_E is the slope of the right straight line of the point e,

$$l_S = \tan(70^\circ) \qquad l_E = \frac{1}{40}. \tag{1}$$

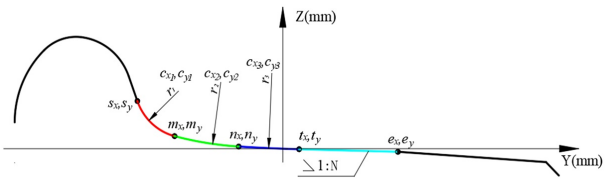

Fig. 1. The expression of the wheel profile.

It is known that three arcs are tangent to each other, and both the red and blue arcs are tangent to the straight lines; thus, the geometry of the wheel profile can be constructed as the radii are determined. First, the centers of the arcs can be derived by Eqs. (2)-(5):

$$c_{y1} = \frac{1}{l_S}(c_{x1} - s_x) + s_y \tag{2}$$

$$(c_{x1} - s_x)^2 + (c_{y1} - s_y)^2 = r_1^2 \tag{3}$$

$$c_{y3} = \frac{1}{l_E}(c_{x3} - t_x) + t_y \tag{4}$$

$$(c_{x3} - t_x)^2 + (c_{y3} - t_y)^2 = r_3^2 \tag{5}$$

where $c_1(c_{x1}, c_{y1})$ and $c_3(c_{x3}, c_{y3})$ are the centers of the 1st and 3rd arcs, respectively, (s_x, s_y) and (t_x, t_y) are the start and end points of the arcs, respectively, and r_1 and r_3 are the radii of the1st and 3rd arcs.

As the centers of the 1st and 3rd arcs are determined, the next step moves to the solution of solving the center of the 2nd arc. To ensure the smoothness of the geometry, which means the first-order derivation of the wheel profile should be continuous mathematically, thus the 2nd arc is tangent to the 1st and 3rd arcs at m (m_x, m_y) and n (n_x, n_y), respectively, which means that the line (c_{x2}, c_{y2}) to (m_x, m_y) and line (c_{x1}, c_{y1}) to (m_x, m_y) are perpendicular to a same tangent line at point m, thus (m_x, m_y), (c_{x2}, c_{y2}) and (c_{x1}, c_{y1}) on a straight line, as well as (n_x, n_y), (c_{x2}, c_{y2}) and (c_{x3}, c_{y3}) share a straight line. Then, we can get:

$$\frac{m_y - c_{y1}}{c_{y1} - c_{y2}} = \frac{m_x - c_{x1}}{c_{x1} - c_{x2}} \tag{6}$$

$$\frac{n_y - c_{y3}}{c_{y3} - c_{y2}} = \frac{n_x - c_{x3}}{c_{x3} - c_{x2}}. \tag{7}$$

Meanwhile, the tangent point (m_x, m_y) on the 1st arc and (n_x, n_y) on the 3rd arc, we can obtain:

$$(m_x - c_{x1})^2 + (m_y - c_{y1})^2 = r_1^2 \tag{8}$$

$$(n_x - c_{x3})^2 + (n_y - c_{y3})^2 = r_3^2. \tag{9}$$

Combining Eqs. (6) and (8), we get:

$$\begin{aligned} &x^2 + \left(\frac{c_{y1} - c_{y2}}{c_{x1} - c_{x2}}\right)^2 x^2 - 2c_{x1}x \\ &-2x \cdot \frac{c_{y1} - c_{y2}}{c_{x1} - c_{x2}} \cdot \left(\frac{c_{y1} - c_{y2}}{c_{x1} - c_{x2}} \cdot c_{x1} - c_{y1}\right) \\ &-2c_{y1}x \cdot \frac{c_{y1} - c_{y2}}{c_{x1} - c_{x2}} + \left(\frac{c_{y1} - c_{y2}}{c_{x1} - c_{x2}} \cdot c_{x1} - c_{y1}\right)^2 \\ &+2c_{y1} \cdot \left(\frac{c_{y1} - c_{y2}}{c_{x1} - c_{x2}} \cdot c_{x1} - c_{y1}\right) + c_{y1}^2 + c_{x1}^2 = r_1^2. \end{aligned} \tag{10}$$

We can obtain a solution of (m_x, m_y) with respect to (c_{x2}, c_{y2}) by solving Eq. (10).

$$m_x = \frac{-b_m + \sqrt{b_m^2 - 4a_m c_m}}{2a_m} \tag{11}$$

$$m_y = \frac{c_{y1} - c_{y2}}{c_{x1} - c_{x2}}(m_x - c_{x1}) + c_{y1} \tag{12}$$

where a_m, b_m and c_m can be solved via quadratic formula. Applying the same process to Eqs. (6) and (8), we can obtain:

$$\begin{aligned} &x^2 + \left(\frac{c_{y3} - c_{y2}}{c_{x3} - c_{x2}}\right)^2 x^2 - 2c_{x3}x \\ &-2x \cdot \frac{c_{y3} - c_{y2}}{c_{x3} - c_{x2}} \cdot \left(\frac{c_{y3} - c_{y2}}{c_{x3} - c_{x2}} \cdot c_{x3} - c_{y3}\right) \\ &-2c_{y3}x \cdot \frac{c_{y3} - c_{y2}}{c_{x3} - c_{x2}} + \left(\frac{c_{y3} - c_{y2}}{c_{x3} - c_{x2}} \cdot c_{x3} - c_{y3}\right)^2 \\ &+2c_{y3} \cdot \left(\frac{c_{y3} - c_{y2}}{c_{x3} - c_{x2}} \cdot c_{x3} - c_{y3}\right) + c_{y3}^2 + c_{x3}^2 = r_3^2. \end{aligned} \tag{13}$$

Then we can obtain the solution of (n_x, n_y) with respect to (c_{x2}, c_{y2}), which is shown in Eqs. (15) and (16):

$$n_x = \frac{-b_n + \sqrt{b_n^2 - 4a_n c_n}}{2a_n} \tag{14}$$

$$n_y = \frac{c_{y3} - c_{y2}}{c_{x3} - c_{x2}}(n_x - c_{x3}) + c_{y3}. \tag{15}$$

Similarly, parameters a_n, b_n and c_n can be solved via quadratic formula. Note that (m_x, m_y) and (n_x, n_y) on 2nd arc, and r_2 is the radius of the 2nd arc, then we can get:

$$(m_x - c_{x2})^2 + (m_y - c_{y2})^2 = r_2^2 \tag{16}$$

$$(n_x - c_{x2})^2 + (n_y - c_{y2})^2 = r_2^2 \tag{17}$$

Finally, combining Eqs. (11), (12), (14)-(17), we can obtain the center coordination of 2nd arc and the tangent points (m_x, m_y), (n_x, n_y)); please note that it is a system of nonlinear equations; four solution sets will be obtained by formula calculation, and we can easily determine a desired solution by considering all the arcs are internally tangent to each other and both the gradient of tangent points m and n are negative.

3. Profile optimization

3.1 Optimization objective

Wheel profile wear is one of the most important factors to restrict the running speed of the train, which not only increases the operation economy and maintaining cost but also impacts the operation safety and riding comfort; serious wheel wear will

further speed up the fatigue of the key components of the vehicle. Lateral acceleration of the bogie is a key factor for running stability of the vehicle, but a poor wheel-rail profile matching due to wheel profile wear enhances the vibration of the frame; large lateral acceleration indicates the shake of the car body, which may cause the derailment of the running vehicle. Lateral force is another important role in ensuring the safety of the running train, especially for the curved line. Therefore, three objectives, including wheel profile wear index, lateral acceleration, and lateral force, are taken as the objectives in this paper.

3.1.1 Objective to reduce wheel profile wear

Wear index, a convenient model to predict wheel/rail wear rates, is given in Eq. (18), where a large wear index indicates the designed profile suffers from a high wear rate during service time. To ensure the optimal wheel profile is of good performance in reducing wear rate, the wear index is introduced to evaluate the wheel profile wear during their service time.

$$W_i = F_{x,i} \cdot \xi_i + F_{y,i} \cdot \eta_i \quad i \in \{L, R\} \tag{18}$$

$$f_1 = \frac{1}{s}\int_t W_L(t) + W_R(t)dt \tag{19}$$

where $F_{x,i}$ and ξ_i are longitudinal creep forces and creepage longitudinal of the *i* wheel profile, respectively, $F_{y,i}$ and η_i are lateral creep forces and creepage lateral of the *i* wheel profile, and L and R indicate the left and right wheel profiles, and s and t are the total running mileage and running time.

3.1.2 Objective to improve stability

Lateral acceleration of the frame is one of key factors for measuring the stability of a running train; an unideal wheel profile will significantly worsen the running stability of a service train, which further affects the safety and comfort of the train. Thus, to improve the stability of the vehicle, the lateral acceleration of the frame is introduced to enhance the stability performance of a running vehicle, which is constructed as follows:

$$f_2 = RMS(Acc_L) \tag{20}$$

where Acc_L is the lateral acceleration of the frame, and RMS indicates the root mean square operation.

3.1.3 Objective to minimize the wheel-rail lateral force

The lateral force is a key factor affecting the derailment coefficient; theoretically, the large lateral force of the wheel will not only cause the phenomenon of derailment, but also cause deformation of the rail track. Thus the wheel-rail lateral force is introduced to evaluate the performance of a wheel profile, which followed by:

$$f_3 = \max\{|F_L|, |F_R|\} \tag{21}$$

where $|F_L|$ and $|F_R|$ are the lateral force of the wheel on the left and right rail track.

To find an optimal wheel profile, three indicators including profile wear index, stability, and lateral force of wheels are taken into account in the objective function, which can be constructed as follows:

$$F = w_1 f_1 + w_2 f_2 + w_3 f_3 \tag{22}$$

where w_1, w_2, and w_3 are the weighting factors for objectives; also, the objective of three indicators should be normalized to eliminate the magnitude of the objectives.

3.2 Constraints

To ensure the designed wheel profiles are reasonable for production, the geometry and dynamics index should be instructed as constraints to improve the performance of the wheel profile.

3.2.1 Geometry constraints

The radius of the arcs should be constrained to avoid two contact points when the curvature of the wheel profile is less than the rail profile.

$$\alpha_i \le r_i \le \beta_i \quad i \in (1,\ 2,\ 3) \tag{23}$$

where α and β are move limits defining the range of the applicability of the radii.

The 3rd arc is tangent to the straight line, and the tangent point (t_x, t_y) is located on the slope, which should be limited as Eq. (24):

$$t_{\min} \le t_x \le t_{\max} \tag{24}$$

where t_{min} and t_{max} are the move limits of the tangent point.

The slope degree *N* is constrained as follows:

$$N_{\min} \le N \le N_{\max} \tag{25}$$

where N_{min} and N_{max} are the moving limits of the slope.

3.2.2 Derailment coefficient constraints

The derailment coefficient is a critical element for evaluating the safety of a running train; thus, the derailment coefficient is adopted as a constraint to ensure the rationality of the wheel profile. The constraint is constructed by Nadal formulation, which is shown in Eq. (26).

$$g_i = \frac{Q}{P} \le \gamma_i \tag{26}$$

where *Q* and *P* are the lateral and normal force of the wheel, respectively, and γ is the limit of the derailment coefficient.

3.3 Vehicle dynamics model

The multibody dynamics software SIMPACK is used to establish a dynamics model, which is constructed with a train body, two frames, four wheelsets and eight axle boxes. The frame and wheelset are connected by the primary suspension, and the frame and train body are connected by the secondary suspension. For the main parameters of the vehicle refer to Ref. [1]. The calculation is conducted assuming the train runs along a railway track with a total length of 2000 m. The first section of the track line was designed with a tangent part of 300 m, a transition part of 200 m, a 1000 m curve part with a radius of 5000 m, and then a transition part of 200 m is connected and the end part is a 300 m tangent line, the measured track irregularity along Changsha-Zhuzhou line is added to the railway track. The superelevation is 100 mm, and the vehicle running speed is set to 250 km/h.

3.4 Kriging-PSO-based optimization

3.4.1 Kriging-based objective function

The Kriging model is a concept arising in reliability theory [28], which can construct a complex surrogate model to approximate original model with a few sampling points. Thus, we utilized a Kriging model to efficiently reduce number of repeated geometry modeling and multibody dynamics simulation. The basic idea of the Kriging model is to use the known input to predict the unknown response. Given the sampling design variables $\mathbf{X} = [x_1, x_2, \ldots, x_n]^T$, $\mathbf{X} \in \Re^{n\times 5}$ which are used for generating candidate wheel profiles, and the corresponding response $\mathbf{Y} = [y_1, y_2, \ldots, y_n]$ with $Y \in \Re^{n\times 1}$ obtained from the multibody simulation, we attempt to construct the Kriging model shown in Eq. (27).

$$\bar{y} = f^T(x)\varphi + \varepsilon(x) \tag{27}$$

where $f^T(x)\varphi$ is a regression model and ε is a stochastic process. The mean error of the random process ε is zero and the covariance between $\varepsilon(x_i)$ and $\varepsilon(x_j)$ is given as:

$$Cov[\varepsilon(x_i), \varepsilon(x_j)] = \sigma^2 R(\theta, x_i, x_j) \tag{28}$$

where $R(\theta, x_i, x_j)$ is the correlation model with parameter θ; the generalized Gauss function is adopted in this paper [28]. Then the maximum likelihood estimation is introduced to evaluate the parameters σ^2 and φ, and the parameter θ can be determined by the least square formulation. Thus, the response of an arbitrary point can be predicted as follows:

$$y(x^*) = f(x^*)\varphi + r(x^*)^T \mathbf{R}^{-1}(\mathbf{Y} - \mathbf{F}\varphi) \tag{29}$$

where R denotes the correlation of all the sampling points, and $r(x^*)$ gives the correlation between sampling design variables and arbitrary point x^*, which is constructed as Eq. (30) [29-31].

$$r(x^*) = [R(x^*, x_1), R(x^*, x_2), \ldots, R(x^*, x_n)]. \tag{30}$$

3.4.2 PSO-based optimization

After constructing the Kriging model for building the relationship between objective function 22 and design variables, the particle swarm optimization method is introduced to find the optimal wheel profile parameters by minimizing the objective Eq. (22). The main idea of the PSO method is to randomly generate a set of particles, and iteratively update the position of the particle to find the optimal design variable for wheel profile. The core step for optimization includes velocity and position update, which is shown in Eqs. (31) and (32) [32–34].

$$v(k+1) = \varpi v(k) + c_1\omega_1(p_d(k) - x(k)) + c_2\omega_2(p_g(k) - x(k)) \tag{31}$$

$$x(k+1) = v(k+1) + x(k) \tag{32}$$

where c_1 and c_2 are learning coefficients, ω_1 and ω_2 are random numbers which lie in the range between 0 and1, p_d and p_g denote the best solution by the particle and swarm, respectively. To improve the convergence performance of the standard PSO method for obtaining the optimal solution, an exponential form of the inertia weight is introduced to accelerate the convergence of the solution, the weight factor ϖ is constructed as follows:

$$\varpi = \lambda_1 \times e^{\left(\lambda_2 \frac{k_{\max} - k_{cur}}{k_{\max}}\right)} \tag{33}$$

where λ_1 and λ_2 are influence factors that determine the range of the weight, and k_{max} and k_{cur} are the maximum and current iterations, respectively.

3.5 Optimization procedure

Based on the aforementioned detailed introduction, the optimization procedure for redesigning the wheel profile is summarized in Fig. 2, which mainly includes six steps:

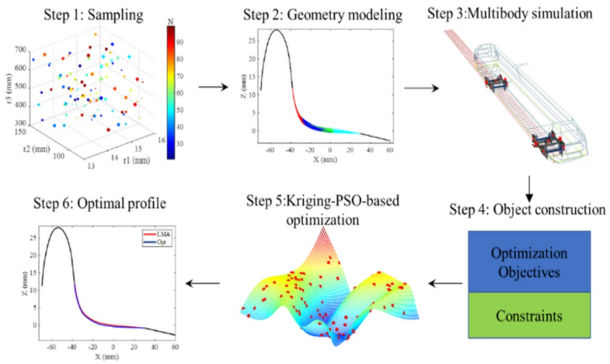

Fig. 2. The flowchart of the wheel profile optimization.

Step 1: Select the design variables matrix **X** with the Latin hypercube sampling strategy.

Step 2: Model the candidate profiles with the geometry modeling method introduced in Sec. 2, and discretize the candidate wheel profile into points with coordinate information which is used as the source of step 3.

Step 3: Construct the multibody simulation model to analyze the dynamics performance of the wheel profiles, and obtain the value of Eqs. (19)-(21) and (26).

Step 4: Evaluate the values of objective function (22), which satisfy the required constraints, and construct response vector **Y**.

Step 5: The Kriging model described in Sec. 3.4.1 is constructed to build the relationship between design variables **X** and corresponding response **Y**, and using the optimization method, PSO described in Sec. 3.4.2, to find the optimal design variables for minimizing the objective function, where the response surface, a sketch map in step 5, is constructed by Kriging surrogate method and the red dots are the initial guess for the optimal solution, which is optimized with PSO method.

Step 6: Reconstruct the optimal wheel profile with the optimal result from step 5 by using the geometry modeling method.

Table 1. The range of the design variables for wheel profile shape.

Design variables	r_1	r_2	r_3	t_x	N
Range (mm)	13-16	80-150	350-700	0-5	20-100

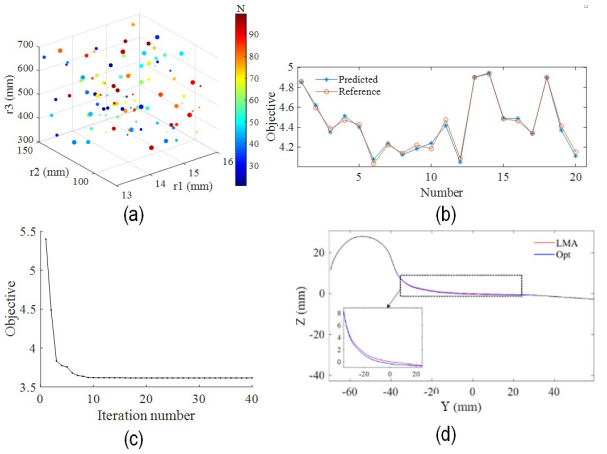

Fig. 3. Metamodel construction and validation: (a) input design variables; (b) metamodel validation; (c) iteration history of the objective function; (d) comparison of LMA and optimal wheel profiles.

4. Numerical results and discussion

In this section, the wheel-rail contact geometry analysis, dynamics response and long-term shape evolution of the wheel profile are considered to fully evaluate the performance of the optimal wheel profile. The dynamics analysis was conducted with the use of SIMPACK. All the algorithms were implemented on the platform MATLAB 2018, and were run on Windows 10, 64 bits, with a 2.9 GHz CPU and 16 GB of RAM.

4.1 Metamodel construction and validation

The Latin hypercube sampling strategy is used to generate candidate profiles, a total of 100 sets of design variables, where the range is given in Table 1, were selected and the weighting factors for objective function were set to 3, 1 and 2, respectively. Learning coefficients c_1, c_2 and influence factors λ_1 and λ_2 in PSO method are 1, 2, 0.5 and 1.2, respectively; the optimization stops if the error of two adjacent optimal solutions smaller than 0.0001 or iterations reach the maximum iteration number 40. Fig. 3(a) shows the input of the design variables, where the color bar gives the distribution of slope degree N and the size of the sampling points indicates the value of t_x, and three coordinate axes indicate the distribution of r_1, r_2 and r_3, respectively.

After constructing the Kriging surrogate model by using a subset (80 sets) of design variables, another 20 sets of design variables are adopted to validate the performance of the metamodel, of which the result is given in Fig. 3(b). We can find that the result of the Kriging-based metamodel is similar to the SIMPACK re-computation solution; the average error of the proposed model is 5.3 %, which indicates the proposed metamodel is of good accuracy for evaluating the response with the input wheel profile parameters.

The iteration history of the objective function is shown in Fig. 3(c). The objective gradually converges as the iteration number increases, and the optimal parameters for wheel profile are (14.6767, 90.9999, 576.4452, 4.5207, 83.5251). Fig. 3(d) compares the geometric shapes of LMA and the optimal wheel profile. It can be found that the newly designed wheel profile is milder at the tread and steeper at the flange than LMA.

4.2 Wheel-rail contact geometry analysis

Contact points are the basis for analyzing the contact mechanics and vehicle dynamics; rational distribution of the wheel-rail contact points leads to good service performance of a running train, such as profile wear distribution and running stability. Figs. 4(a) and (b) show the distribution of contact points on the wheel and rail based on various lateral displacements. We observe that the contact points on the optimal wheel profile shape are as uniform as the LMA wheel profile; meanwhile, the contact width on the optimal wheel profile is 2.3 mm wider than the LMA profile, and corresponding contact width on the rail increases 3.9 mm, which indicates the wear on the optimal wheel profile will present wider and more uniform than the LMA profile. Subplots (c) and (d) compare the equivalent conicity and rolling radius difference of the LMA wheel profile and the optimal one. We find that the equivalent conicity of the optimal wheel profile is lower than the LMA profile when the lateral displacement is within 8 mm, which guarantees the optimal wheel profile a higher running speed on the tangent route. A large equivalent conicity of the wheel profile guaran-

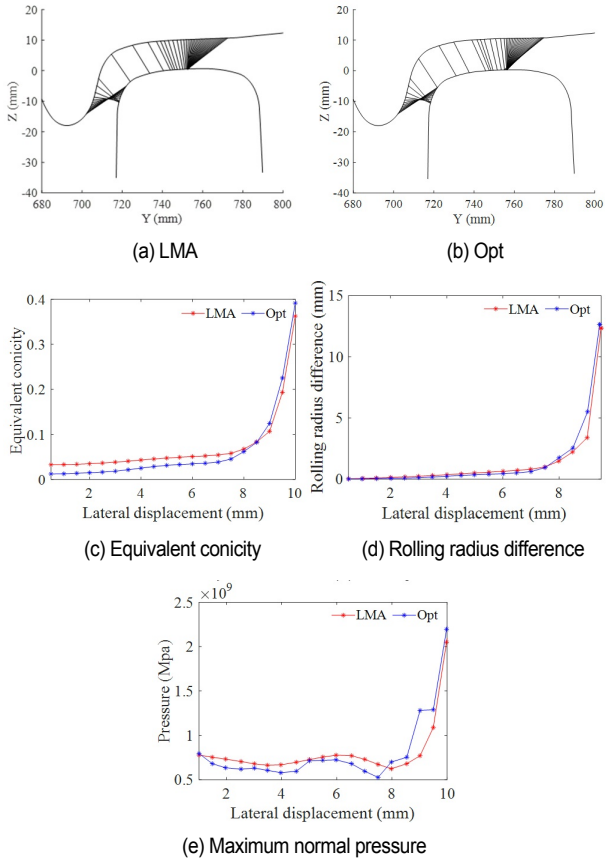

(a) LMA (b) Opt

(c) Equivalent conicity (d) Rolling radius difference

(e) Maximum normal pressure

Fig. 4. The contact distribution, equivalent conicity, rolling radius difference, and the maximum normal pressure of the LMA and optimal shape.

tees the characteristic of curve negotiation. We find that the equivalent conicity of the optimal one is higher than the LMA profile when the lateral displacement is over 8 mm, which indicates the optimal wheel profile is of better property of curve negotiation. Subplot (e) gives the maximum normal pressure of the wheel profile contacting with CN 60 rail under various lateral displacements. We find that the maximum normal pressure of the optimal wheel profile is lower than the LMA on the main contact area, which leads to low contact pressure between the wheel and rail and reduces the wear and fatigue of the wheel to some extent.

4.3 Dynamics performance

To demonstrate the service performance of the optimal wheel profile, a dynamics analysis of the train was conducted on the tangential and curve lines, respectively. Therefore, the lateral acceleration of the bogie, derailment coefficients, lateral force of the wheelset, and the wear index were introduced as indicators to analyze the dynamics performance of the wheel geometric shape. Two types of tracks, tangent and curve lines, were constructed for evaluating vehicle dynamics performance. The tangent line is a straight line without any curve or superelevation and the curved line, for some particular operating

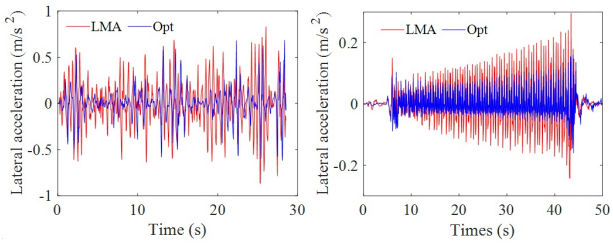

(a) Tangential line (b) Curve line

Fig. 5. Lateral acceleration of the bogie on the tangential and curved lines, respectively.

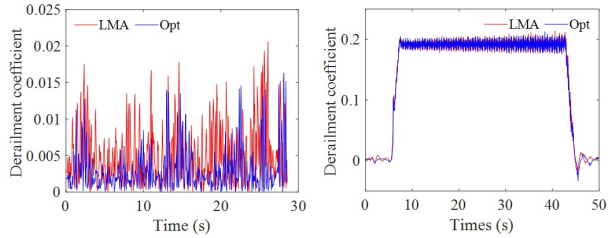

(a) Tangential line (b) Curve line

Fig. 6. Derailment coefficient on the tangential and curved lines.

cases, is constituted of two tangent parts of 100 m, two transition parts of 50 m, and a 700 m curve part with a radius of 1000 m, of which the superelevation of the curve part is 60 mm, and measured track irregularity is added for both the tangent and curve lines. To reflect the most operation cases of the served high-speed train, the speed of the vehicle on the tangent was set to 250 km/h, and curved lines were set to 72 km/h.

The lateral acceleration of the bogie affects the running stability of the train at a high speed. Fig. 5 compares the lateral acceleration of the bogie when using the LMA and the optimal wheel profile on the tangential and curve lines, respectively. It can be observed that the lateral acceleration of the bogie when using the LMA and the optimal wheel profile on the tangential line is 0.8663 and 0.6840 m/s^2, respectively. The root mean square of two wheels is 0.1773 and 0.1026, respectively, in which the optimal wheel profile decreases 42.13 % compared to the LMA. On the curve line, the maximum lateral acceleration of the LMA and optimal wheel profile is 0.2956 and 0.1597 m/s^2, respectively. The root mean square of the LMA and optimal wheel shape are 0.0774 and 0.0455, respectively; the acceleration of the optimal result decreases 41.21 % compared with the LMA profile. Therefore, the optimal wheel profile performs better than the LMA wheel profile both on the tangential and the curve lines from the perspective of the lateral acceleration, which improves the running stability of the train.

The derailment coefficient of the train directly relates to the running safety of the train; a well-designed wheel profile will keep the running train in a reliable situation. Thus, we compared the derailment coefficient of the wheel when using LMA and the optimal wheel profile, which is presented in Fig. 6. From subplot (a), we find that the derailment coefficient of the

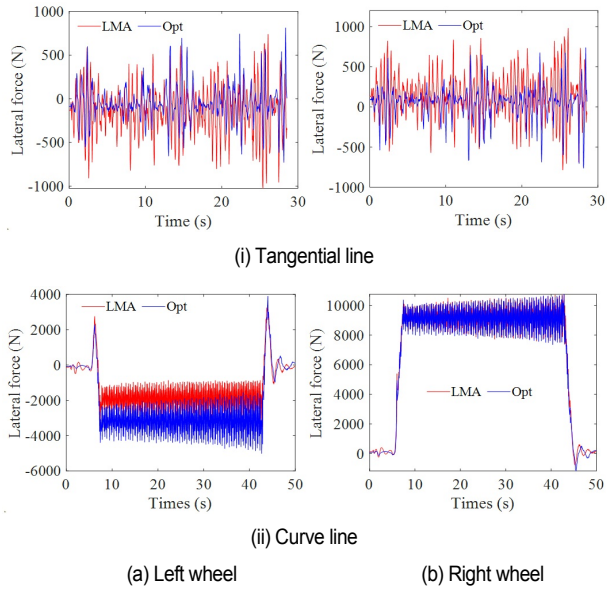

Fig. 7. Lateral force of the left and right wheel on the curved line.

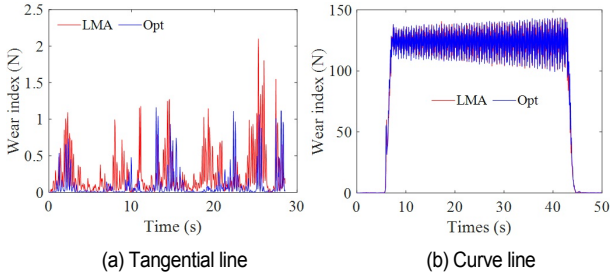

Fig. 8. Wear index of the wheelset.

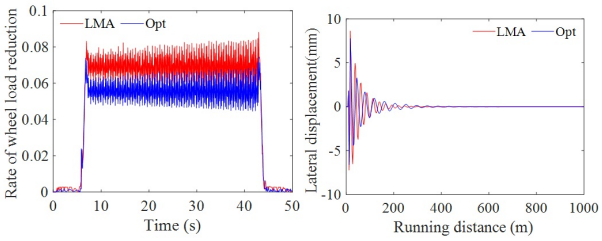

Fig. 9. Running stability of the wheel profile: (a) rate of wheel load reduction; (b) lateral displacement of the wheelset.

LMA and the optimal wheel profile on the tangential line are 0.0206 and 0.0163, respectively, in which the optimal wheel profile decreases 20.79 % compared to the LMA profile. On the curved line, the derailment coefficient of the LMA and the optimal profile are 0.2137 and 0.2127, respectively, which indicates the optimal wheel profile performs as well as the LMA. Thus, we find the optimal wheel profile improves the running safety of the train.

The lateral force of the wheelset is another factor related to the running stability of the train; a large lateral force not only results in large wheel-rail wear, but also may cause surface fatigue and derailment of the wheel. Thus, the maximum lateral force of the wheel should be limited to ensure a good running performance of the train. Fig. 7 gives the lateral force of the wheelset on the tangential and curved lines; from the first row, it can be found that the maximum lateral force of the left wheel of the LMA and the optimal one is 1023.58 N and 811.91 N, respectively, and the right wheel is 979.783 N and 763.843 N, where the maximum lateral force of optimal wheel profile decreases 20.72 % more than the LMA shape. The second row shows the lateral force of the wheelset on the curved line; the maximum lateral force of the left wheel when using LMA and the optimal wheel profile is 3870.9 N and 5014.3 N, respectively, and the right wheel of the LMA and the optimal one are 10720.2 N and 10749.5 N, respectively. Though the lateral force of the left wheel is larger when using the optimal wheel profile, the difference between the right and left wheels is smaller than the one of the LMA profile, which indicates the optimal wheel profile is safer than the LMA wheel profile.

Fig. 8 shows the wear index of the wheels running on the tangential and curved lines. When the vehicle runs on the tangential line, the average wear index of the LMA and the optimal wheel profile are 0.2219 and 0.0888, respectively, in which the wear index of the optimal geometric shape decreases 59.98 % when compared with the LMA wheel. As for the curved line, the average wear index of the LMA and the optimal wheel profile are 92.10 and 92.02, respectively. We find that the optimal wheel profile performs better than the LMA on the tangential line, and as well as LMA wheel profile on the curved line.

To further evaluate the curve passing performance of the optimized wheel profile, the rate of wheel load reduction is presented in Fig. 9(a). We find that both the LMA profile and the optimized wheel profile have good performance on curve passing; the maximum rate of wheel load reduction of LMA and the optimized one is 0.088 and 0.075, respectively, and the optimized wheel profile performs better than classic LMA wheel profile. Subplot (b) shows the lateral displacement of the wheelset when the vehicle runs on a tangent track and passes a lateral sinusoidal irregularity excitation at a speed of 250 Km/h. We find that both the LMA and optimized wheel profile can smoothly pass the excitation and the lateral displacement curve will converge to zero eventually, due to the equivalent conicity of the optimized wheel profile being smaller than LMA wheel profile; thus, the optimized wheel profile needs slightly longer time to converge.

Overall, we find that the optimal wheel profile performs better than the LMA profile on the tangential line by comparing the lateral acceleration, derailment coefficients, lateral force and wear index of wheels. As for the curved line, the optimal wheel profile performs as well as the LMA wheel profile. To some extent the stability of the optimal wheel is better than the LMA wheel shape. Therefore, it can be concluded that the optimal wheel profile has good performance.

4.4 Long-term profile wear analysis

Physics-driven wheel profile wear evolution is an effective method for analyzing the service performance of the newly designed wheel profile. We introduced a long-term profile wear prediction model combining vehicle dynamics analysis, contact mechanics, and material removal model to analyze the wear of the wheel profile, where the normal and tangential stress are determined by Hertz and FASTSim methods, respectively, and the Archard model is used to evaluate the material removal of the wheel profile. The track is constituted of two 1500 m tangent parts and 500 m transition parts as well as a 1000 m curved part of a radius of 5000 m; the superelevation is 100 mm and vehicle speed is set to 250 km/h.

The long-term profile wear evolution performance of LMA and the optimal wheel profile was evaluated at various service stages, which is shown in Fig. 10. The maximum wear depth of the wheel profile is summarized in Table 2. Both the wear depth and wear area increase as the mileage increases; the wear on the left wheel is mainly focused on the rolling contact circle, and the main wear area of the right wheel is mainly focused on the abscissa around 12. Meanwhile, the wear of both the left and right wheels of the LMA wheel profile is more severe than the optimal wheel profile at every service stage. The maximum wear depth of the optimal wheel profile averagely decreases over 10 %; thus, the optimal wheel profile has good performance in wheel profile wear evolution.

Table 2. The maximum wear depth of the left and right wheel profiles under various stages (mm).

Stage		40000 km	80000 km	120000 km	160000 km
LMA	Left	0.24	0.46	0.66	0.86
Opt		0.20	0.35	0.57	0.78
LMA	Right	0.30	0.52	0.72	0.92
Opt		0.24	0.44	0.65	0.86

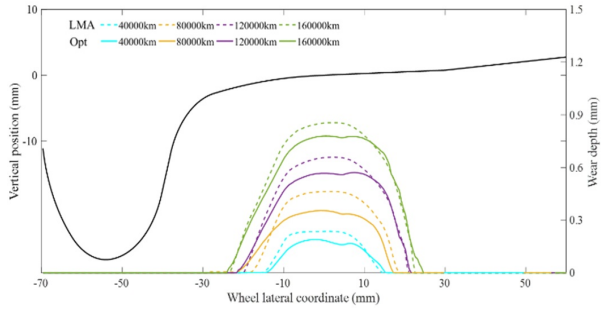

(a)

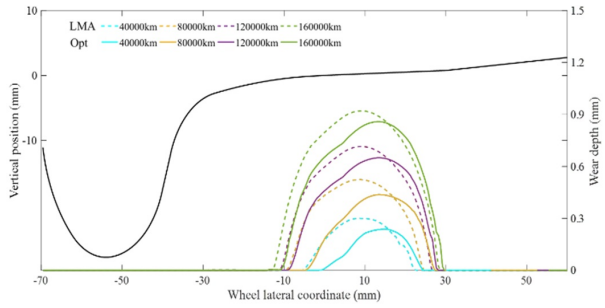

(b)

Fig. 10. The long-term wheel profile evolution: (a) the left wheel profile; (b) the right wheel profile.

To further evaluate the dynamics performance of the long-term worn wheel profile, the lateral acceleration of the bogie and the derailment coefficient of the worn wheel profile after running 160000 km were assessed, and band-pass filtering was applied to acceleration data according to Ref. [35], with the comparison presented in Fig. 11. We find that the dynamics performance of the worn LMA wheel profile is worse than the optimal wheel profile; the root mean square of the lateral acceleration of the LMA and optimal wheel profile was 3.3114 and 2.4716, respectively; the maximum derailment coefficient of the worn LMA wheel profile was 0.56, which is greater than the optimal wheel profile 0.15.

4.5 Discussion and future work

The proposed pipeline combining the Kriging surrogate model and particle swarm optimization for wheel profile optimization can effectively and efficiently design a wheel profile considering multiple objectives.

First, the weights used in the objective function of this paper are solely for validating the effectiveness of the wheel profile optimization pipeline, and we apply a relatively large weight to reduce profile wear in this paper. However, readers can adjust the weights of the objective function to achieve good performance with other indicators. Moreover, we have to address that, as demonstrated by Hertz theory, the shape difference of wheels and rails significantly impacts the wheel-rail contact, which directly affects the normal pressure shown in Fig. 4(e) and the normal and lateral force. We observe that the optimized wheel profile shown in Fig. 3(d) is slightly steeper than the LMA profile at the area near to wheel flange, which causes the difference of the lateral force of the Opt and LMA profiles. The derailment coefficient shown in Fig. 6 is related to both the normal and lateral force, and the normal force changes as the lateral force changes; as indicated in Eq. (26), the value of

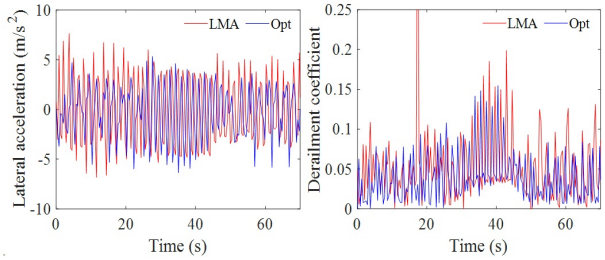

(a) Lateral acceleration (b) Derailment coefficient

Fig. 11. The dynamics performance of the worn wheel profile.

derailment coefficient is normal force over lateral force, so the derailment coefficients of the Opt and LMA are similar. Similarly, the wear index shown in Fig. 8 depends on creep forces and creepage of both the left and right wheels; the resultant of the creep forces and creepage of the LMA and Opt wheel profiles is almost the same to some extent.

Second, this method is not limited to optimizing the geometric shape for high-speed train, but it can be applied to design the wheel profile for metro and freight trains. Additionally, there are many choices to establish an objective function with multiple constraints. We selected commonly used objectives, including wear and stability indicators for wheel profile design in this paper, and we introduced geometry and derailment coefficient constraints to ensure a suitable wheel-rail contact relationship and running safety, respectively. We have to address that the practical application of wheel profile optimization is a complicated engineering problem; many factors such as dynamical loads, track irregularity, lubrication conditions of wheel rail surface affect the vehicle system dynamics and wheel profile evolution. The selection of the objective function and constraints is important in engineering application, in which the practical working conditions should be comprehensively considered in the process of wheel shape design. The proposed wheel profile design framework is not limited to optimizing the geometric shape for improving the wear and stability indicators. The objective functions and constraints can be altered to design a wheel profile for various working conditions in practice.

Third, not only the geometric shape of the wheel tread affects the wear distribution and vehicle dynamics, but also the wheel plate has an impact on the self-excited vibration of a wheel-rail system, which further affects the wheel-rail profile wear evolution. Thus, shape and topology optimization of the wheel plate can be conducted to improve the dynamic performance of the wheel by using lattice structure and honeycomb structure [36-38]. Furthermore, simultaneous optimization of wheel shape and vehicle dynamics parameters is an important topic in practical application, and other optimization methods such as Taguchi optimization [39] can also be further studied in wheel profile optimization instead of Kriging-PSO optimization framework in future.

5. Conclusions

This paper proposes a shape optimization pipeline for the wheel profile of the high-speed train. We first introduced the parametric geometry modeling method for the wheel shape to generate numerous candidate profiles, and conducted multi-body simulation to analyze the dynamics response of the wheel profile. To construct the response model between the geometric parameters and the dynamics response, the Kriging approximation model was introduced to reduce the number of simulation runs. Finally, the weighted particle swarm optimization method was employed to find the optimal wheel profile, and the dynamic analysis was conducted to evaluate the wheel-rail interaction performance. The numerical result shows that the optimized wheel profile is of good performance at the design stage, of which the lateral acceleration, derailment coefficient, maximum lateral force and wear index of the new designed profile are decreased when compared with the LMA wheel profile on the tangential line, and is of comparable performance on the curve line. Further investigation on the long-term profile wear evolution shows the optimized wheel profile is of better performance, including wear depth and dynamics response than the LMA wheel profile.

Acknowledgments

This work was supported by the National Natural Science Foundation of China, grant number 51975589, Zhejiang Provincial Natural Science Foundation of China, grant number LY21E050008, Ningbo Key research and development Program, grant number 2023Z134, and the first author was funded by China Scholarship Council.

References

[1] D. Cui, R. Wang, P. Allen, B. An, L. Li and Z. Wen, Multi-objective optimization of electric multiple unit wheel profile from wheel flange wear viewpoint, *Structural and Multidisciplinary Optimization*, 59 (1) (2019) 279-289.

[2] D. Chen, G. Sun, L. Xing, Y. Wu and G. Shen, A grinding profile design method for rails in the switch area considering a representative set of wheel profiles. *J. of Mechanical Science and Technology*, 37 (10) (2023) 4923-4933.

[3] H. Y. Choi, D. H. Lee and J. Lee, Optimization of a railway wheel profile to minimize flange wear and surface fatigue, *Wear*, 300 (1-2) (2013) 225-233.

[4] J. Shi, Y. Gao, X. Long and Y. Wang, Optimizing rail profiles to improve metro vehicle-rail dynamic performance considering worn wheel profiles and curved tracks, *Structural and Multidisciplinary Optimization*, 63 (1) (2021) 419-438.

[5] S. Zakharov, I. Goryacheva, V. Bogdanov, D. Pogorelov, I. Zharov, V. Yazykov, E. Torskaya and S. Soshenkov, Problems with wheel and rail profiles selection and optimization, *Wear*, 265 (9-10) (2008) 1266-1272.

[6] M. Novales, A. Orro and M. R. Bugarín, Use of a genetic algorithm to optimize wheel profile geometry, *Proceedings of the Institution of Mechanical Engineers, Part F: J. of Rail and Rapid Transit*, 221 (4) (2007) 467-476.

[7] D. Cui, H. Wang, L. Li and X. Jin, Optimal design of wheel profiles for high-speed trains, *Proceedings of the Institution of Mechanical Engineers, Part F: J. of Rail and Rapid Transit*, 229 (3) (2015) 248-261.

[8] V. L. Markine, I. Y. Shevtsov and C. Esveld, An inverse shape design method for railway wheel profiles, *Structural and Multidisciplinary Optimization*, 33 (3) (2007) 243-253.

[9] I. Y. Shevtsov, V. L. Markine and C. Esveld, Design of railway wheel profile taking into account rolling contact fatigue and wear, *Wear*, 265 (9-10) (2008) 1273-1282.

[10] H. Jahed, B. Farshi, M. A. Eshraghi and A. A. Nasr, Numerical optimization technique for design of wheel profiles, *Wear*, 264 (1-2) (2008) 1-10.

[11] G. Shen, J. B. Ayasse, H. Chollet and I. Pratt, A unique design method for wheel profiles by considering the contact angle function, *Proceedings of the Institution of Mechanical Engineers, Part F: J. of Rail and Rapid Transit*, 217 (1) (2003) 25-30.

[12] D. Ren, G. Tao, Z. Wen and X. Jin, Wheel profile optimisation for mitigating flange wear on metro wheels and verification through wear prediction, *Vehicle System Dynamics*, 59 (12) (2021) 1894-1915.

[13] O. Polach, Wheel profile design for target conicity and wide tread wear spreading, *Wear*, 271 (1-2) (2011) 195-202.

[14] L. Li, D. Cui and X. Jin, State of arts of the study on railway wheel profile optimization, *J. of Southwest Jiaotong University*, 44 (1) (2009) 810-816.

[15] D. Cui, L. Li, X. Jin and X. Li, Optimal design of wheel profiles based on weighed wheel/rail gap, *Wear*, 271 (1-2) (2011) 218-226.

[16] J. Zhang, Z. Wen and L. Sun, Wheel profile design based on rail profile expansion method, *Chinese J. of Mechanical Engineering*, 44 (3) (2008) 44-49.

[17] Y. Qi, H. Dai, P. Wu, F. Gan and Y. Ye, RSFT-RBF-PSO: a railway wheel profile optimisation procedure and its application to a metro vehicle, *Vehicle System Dynamics*, 60 (10) (2021) 1-21.

[18] F. Lin, S. Zhou, X. Dong, Q. Xiao, H. Zhang, W. Hu and L. Ke, Design method of LM thin flange wheel profile based on NURBS, *Vehicle System Dynamics*, 59 (1) (2021) 17-32.

[19] Y. Ye, J. Vuitton, Y. Sun and M. Hecht, Railway wheel profile fine-tuning system for profile recommendation, *Railway Engineering Science*, 29 (1) (2021) 74-93.

[20] D. Cui, H. Wang, L. Li and X. Jin, Optimal design of wheel profiles for high-speed trains, *Proceedings of the Institution of Mechanical Engineers, Part F: J. of Rail and Rapid Transit*, 229 (3) (2015) 248-261.

[21] Y. Ye, Y. Qi, D. Shi, Y. Sun, Y. Zhou and M. Hecht, Rotary-scaling fine-tuning (RSFT) method for optimizing railway wheel profiles and its application to a locomotive, *Railway Engineering Science*, 28 (2020) 160-183.

[22] Y. Ye, Y. Sun, S. Dongfang, D. Shi and M. Hecht, Optimizing wheel profiles and suspensions for railway vehicles operating on specific lines to reduce wheel wear: a case study, *Multibody System Dynamics*, 51 (2021) 91-122.

[23] H. Yamashita, C. Feldmeier, Y. Yamazaki, T. Kato, T. Fujimoto, O. Kondo and H. Sugiyama, Wheel profile optimization procedure to minimize flange wear considering profile wear evolution, *Proceedings of the Institution of Mechanical Engineers, Part F: J. of Rail and Rapid Transit*, 236 (6) (2022) 672-683.

[24] B. Liu, T. X. Mei and S. Bruni, Design and optimisation of wheel–rail profiles for adhesion improvement, *Vehicle System Dynamics*, 54 (3) (2016) 429-444.

[25] W. Ren, L. Li, D. Cui and G. Chen, An improved parallel inverse design method of EMU wheel profile from wheel flange wear viewpoint, *Shock and Vibration*, 2021 (2021) 1-15.

[26] F. Lin, X. Dong, Y. Wang and C. Ni, Multiobjective optimization of CRH3 EMU wheel profile, *Advances in Mechanical Engineering*, 7 (1) (2015) 284043.

[27] R. Chen, C. Hu, J. Xu, P. Wang, J. Chen and Y. Gao, An innovative and efficient method for reverse design of wheel-rail profiles, *Applied Sciences*, 8 (2) (2018) 239.

[28] B. Echard, N. Gayton and M. Lemaire, AK-MCS: an active learning reliability method combining Kriging and monte carlo simulation, *Structural Safety*, 33 (2) (2011) 145-154.

[29] Y. Feng, L. Xin, J. Hao, N. Ding and F. Wang, Numerical simulation of long-span bridge response under downburst: parameter optimization using a surrogate model, *Mathematics*, 11 (2023) 1-23.

[30] Y. Gao and X. Wang, An effective warpage optimization method in injection molding based on the Kriging model, *The International J. of Advanced Manufacturing Technology*, 37 (9) (2008) 953-960.

[31] W. Li, R. Yang, Q. Qi, Q. Dong and G. Zhao, A novel structural reliability method based on active Kriging and weighted sampling, *J. of Mechanical Science and Technology*, 35 (6) (2021) 2459-2469.

[32] L. Bo, Z. Zhang, Y. Liu, S. Yang, Y. Wang, Y. Wang and X. Zhang, Research on path planning method of solid backfilling and pushing mechanism based on adaptive genetic particle swarm optimization, *Mathematics*, 12 (3) (2024) 1-27.

[33] A. Onat and P. Voltr, Particle swarm optimization based parametrization of adhesion and creep force models for simulation and modelling of railway vehicle systems with traction, *Simulation Modelling Practice and Theory*, 99 (2020) 102026.

[34] B. Nautiyal, R. Prakash, V. Vimal, G. Liang and H. Chen, Improved salp swarm algorithm with mutation schemes for solving global optimization and engineering problems, *Engineering with Computers*, 38 (2022) 3927-3949.

[35] GB/T 5599-2019, *Specification for Dynamic Performance Assessment and Testing Verification of Rolling Stock*, The Standardization Administration of the People's Republic of China, China (2019).

[36] S. Akıncıoğlu, Taguchi optimization of multiple performance characteristics in the electrical discharge machining of the TiGr2, *Facta Universitatis, Series: Mechanical Engineering*, 20 (2) (2022) 237-253.

[37] F. Wu, H. Lian, G. Pei, B. Guo and Z. Wang, Design and optimization of the variable-density lattice structure based on load paths, *Facta Universitatis, Series: Mechanical Engineering*, 21 (2) (2023) 273-292.

[38] L. Liu, B. Yi, T. C. Wang, Z. Z. Li, J. Zhang and G. H. Yoon, Investigation on numerical analysis and mechanics experiments for topology optimization of functionally graded lattice structure, *Additive Manufacturing*, 47 (2021) 1-8.

[39] B. Safaei, E. C. Onyibo, M. Goren, K. Kotrasova, Z. Yang, S. Arman and M. Asmael, Free vibration investigation on RVE of proposed honeycomb sandwich beam and material selection optimization, *Facta Universitatis, Series: Mechanical Engineering*, 21 (1) (2023) 31-50.

Bing Yi is an Associate Professor of School of Traffic and Transportation Engineering, Central South University, Changsha, China. He received his Ph.D. in Mechanical Engineering from Zhejiang University. He was a research fellow in the Department of Mechanical Engineering at University of Michigan from 2017 to 2019. His research interests include railway engineering, shape and topology optimization, and virtual reality.